Chinese Chemical Letters 37 (2026) 111534

Contents lists available at ScienceDirect

Chinese Chemical Letters

journal homepage: www.elsevier.com/locate/cclet

Post-metalation of thiacalix[4]arene-supported octahedral Co_{24} coordination cage for visible-light photothermal conversion

Yinjuan Guo[a], Dongao Mao[a], Kun Zhou[a], Baokuan Chen[a], Yanfeng Bi[a,*], Xinxin Hang[b,*]

[a] School of Petrochemical Engineering, Liaoning Petrochemical University, Fushun 113001, China
[b] Institute for Innovative Materials and Energy, School of Chemistry and Chemical Engineering, Yangzhou University, Yangzhou 225002, China

ARTICLE INFO

Article history:
Received 6 June 2025
Revised 26 June 2025
Accepted 2 July 2025
Available online 2 July 2025

Keywords:
Coordination cages
Post-synthetic metalation
Metal nanoparticles
Thiacalixarene
Photothermal conversion

ABSTRACT

The conjugation of metal-organic architectures with metal nanoparticles into a multicomponent system is an attractive route for designing myriad materials with structural complexity, integrated properties, and important applications. Herein, we report a single-crystal to single-crystal transition from the thiacalixarene-based octahedral coordination cage Co_{24}-Na to Co_{24}-Ag and the construction of nanohybrids (Co_{24}-Ag@Ag-NPs) by combining Co_{24}-Ag with silver nanoparticles (Ag NPs) for photothermal conversion. The multicomponent Co_{24}-Ag@Ag-NPs not only combined and enhanced the light absorption effect of Co_{24}-Ag and the plasmon effect of Ag NPs but also offered the Mott-Schottky heterojunction. Benefiting from the improved photo-response ability and the protective effect of calixarene in preventing heat loss, Co_{24}-Ag@Ag-NPs exhibited significant visible light photothermal conversion performance.

© 2026 Published by Elsevier B.V. on behalf of Chinese Chemical Society and Institute of Materia Medica, Chinese Academy of Medical Sciences.

Metal-organic coordination cages (MOCCs) [1,2] formed by the self-assembly of metal/metal-cluster nodes and organic spokes are being explored for various applications in catalysis [3–5], biological applications [6,7], separation [8,9], energy conversion [10,11], *etc.* [12,13]. Generally, the properties and functionalities of such MOCCs depend on the components used in their construction as well as their spatial arrangement [14,15]. As indispensable components of MOCCs, metal centers are vital for dictating their structural diversity and functionality. In this context, tailoring specific metal nodes is immensely valuable for the function modulation of MOCCs, but it remains challenging in terms of synthesis. On the other hand, combining multiple components into nanohybrids allows materials to exhibit compositional complexity, multiple integrated functionalities, and various applications beyond their constituents [16–18]. MOCCs featuring well-defined cage structures are ideal platforms for the synthesis of various multicomponent systems owing to their guest-accessible pores, modularity, and versatile chemistry. The integration of MOCCs with special components, such as metal complexes [19], metal-organic frameworks (MOFs) [20], polyoxometalates (POMs) [21], and metal nanoparticles (MNPs) [22], has been recognized as an effective strategy for producing hybrids with multi-functionality and high performance.

Thiacalixarenes, especially *p-tert*-butylthiacalix[4]arene (H_4TC4A) and its derivative *p-tert*-butylsulfonylcalix[4]arene (H_4TC4A-SO_2), have been documented for the construction of metal-organic architectures with high thermal/chemical stability and strong structural rigidity because their multiple pre-organized coordination sites easily bind metal ions to form modular polynuclear secondary building units (PSBUs) [23–26]. In recent years, significant efforts and achievements have been made in the fields of thiacalixarene-based porous coordination cages [27–31], high-nuclearity metal clusters [32–35], and multi-dimensional networks [36,37]. Very recently, thiacalixarene-based metal clusters, especially Cu and Ag clusters, have been recognized as promising photothermal materials owing to their enhanced light absorption effect and nonradiative migration-triggered photothermal conversion behaviour [38–40]. In addition, plasmonic MNPs can produce a local surface plasmon resonance effect under specific irradiation, leading to strong light absorption, thus demonstrating remarkable photothermal and photoelectronic responses [41–43]. Therefore, the conjugation of thiacalixarene-based metal clusters with plasmonic MNPs may promote the construction of hybrids in addition to their photothermal conversion ability.

Motivated by the above prospects, a concept that integrates a thiacalixarene-based metal cluster (Co_{24}-Ag) with Ag NPs was implemented in this study to boost the photothermal conversion performance. The nanohybrid Co_{24}-Ag@Ag-NPs was constructed by post-synthetic metalation of a pre-synthesized thiacalixarene-based Co_{24}-Na cluster undergoing a single-crystal to single-crystal

* Corresponding authors.
E-mail addresses: biyanfeng@lnpu.edu.cn (Y. Bi), hangxinxin@yzu.edu.cn (X. Hang).

https://doi.org/10.1016/j.cclet.2025.111534
1001-8417/© 2026 Published by Elsevier B.V. on behalf of Chinese Chemical Society and Institute of Materia Medica, Chinese Academy of Medical Sciences.

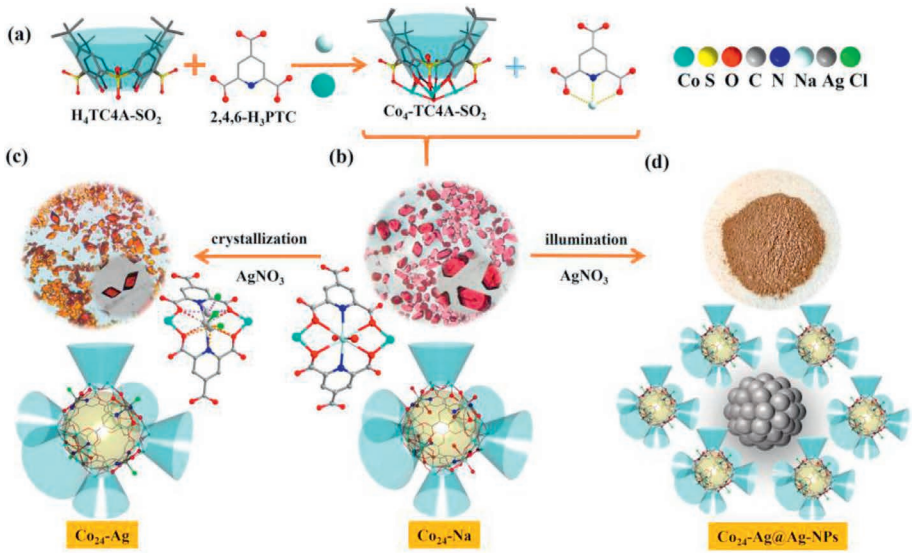


Fig. 1. Schematic illustration of the synthesis strategy for Co_{24}-Na, Co_{24}-Ag, and Co_{24}-Ag@Ag-NPs. (a, b) Co_{24}-Na (red crystals) self-assembled from $H_4TC4A\text{-}SO_2$, 2,4,6-H_3PTC, and Co^{2+}, in the presence of Na^+. (b, c) Single-crystal-to-single-crystal transition from Co_{24}-Na to Co_{24}-Ag (brown crystals). (b, d) Co_{24}-Ag@Ag-NPs (brown powder) obtained from ion exchange of Co_{24}-Na with $AgNO_3$ accompanied by illumination.

transition, followed by illumination. Taking advantage of the enhanced light adsorption effect of Co_{24}-Ag, the local surface plasmon resonance effect of Ag NPs, as well as the Mott-Schottky heterojunction from Co_{24}-Ag and Ag NPs, Co_{24}-Ag@Ag-NPs exhibit superior photothermal conversion ability both in solid state and in organic solution.

As illustrated in Fig. 1, the Co_{24}-Na cluster was successfully self-assembled *via* the solvothermal reaction of $Co(Ac)_2{\cdot}4H_2O$, $H_4TC4A\text{-}SO_2$, pyridine-2,4,6-tricarboxylic acid (2,4,6-H_3PTC), and NaCl in a mixed solvent of CH_3OH-DMF at 130 °C for 72 h. The Co_{24}-Ag cluster was obtained when a CH_2Cl_2 solution of Co_{24}-Na was treated with $AgNO_3$ in CH_3CH_2OH at ambient conditions for 12 h (Scheme S1 in Supporting information).

Single-crystal X-ray diffraction (SCXRD) analysis revealed that Co_{24}-Na has an octahedral cluster structure [44], wherein six Co_4-($TC4A\text{-}SO_2$) PSBUs are connected by eight 2,4,6-PTC auxiliary linkers (Fig. S1 in Supporting information) and four Na^+ ions are fixed on the surface by two carboxyl oxygen donors and two head-to-head nitrogen atoms (Fig. 1b). Co_{24}-Ag is consistent with the crystal structure of Co_{24}-Na, except for the axial coordination sites (Fig. 1c). In Co_{24}-Na, two water molecules occupy the two axial coordination sites of Na^+ (Fig. 1b), whereas each Ag^+ is disordered into three parts (Fig. S1e in Supporting information) in Co_{24}-Ag bonds to the *in situ* generated Cl^- anion (C–Cl bond cleavage of CH_2Cl_2) in the axial direction (Fig. 1c) [38,45–47]. The capped oxygen atoms at the bottom of the PSBU were assigned to four OH^- (O18*) and two H_2O (O19*) in Co_{24}-Na and transferred to six H_2O (O21*) in Co_{24}-Ag after the ion exchange experiment. The assignment of these species is based on symmetry considerations, BVS calculations (Tables S2 and S3 in Supporting information), and overall charge balance considerations, which are also familiar in $TC4A\text{-}SO_2$-based coordination cages/clusters [26,48]. Powder X-ray diffraction (PXRD) investigations indicated that bulk Co_{24}-Na and Co_{24}-Ag crystal patterns matched well with those simulated from SCXRD (Figs. S2 and S3 in Supporting information). Fourier transform infrared (FT-IR) spectra illustrated that the functional groups showed no significant changes (Fig. S4 in Supporting information), suggesting that the ion exchange process did not disturb the original structure. Matrix-assisted laser desorption ionization time-of-flight mass spectroscopy (MALDI-MS) was used further to verify the formation of Co_{24}-Na and Co_{24}-Ag clusters. The MALDI-MS spectra of Co_{24}-Na in CH_3OH and Co_{24}-Ag in CH_2Cl_2 show the prominent peak located at 8808.74 and 8999.27 Da, which can be assigned to $[Co_{24}(H_2O)_2(OH)_4(TC4A\text{-}SO_2)_6(2,4,6\text{-}PTC)_8Na_4(H_2O)_8]+(CH_3OH)_{10}$ and $[Co_{24}(H_2O)_6(TC4A\text{-}SO_2)_6(2,4,6\text{-}PTC)_8Ag_4Cl_4]+(CH_2Cl_2)_2$ species, respectively (Fig. S5 in Supporting information). The thermal stabilities of Co_{24}-Na and Co_{24}-Ag and the residual species after thermogravimetric (TG) experiments were analyzed by TG and PXRD, respectively (Figs. S6-S9 in Supporting information). TG analysis revealed that both Co_{24}-Na (Fig. S6 in Supporting information) and Co_{24}-Ag (Fig. S8 in Supporting information) contain additional disordered solvents besides SCXRD determination, whose contributions were identified by the SQUEEZE method in PLATON (see Supporting information for details). The PXRD data showed definite Ag species in the thermogravimetric residue of Co_{24}-Ag (Fig. S9 in Supporting information) compared with that of Co_{24}-Na (Fig. S7 in Supporting information).

X-ray photoelectron spectroscopy (XPS) measurements were performed to analyze the differences in the coordination environment of the metal ions in the obtained Co_{24}–Na and Co_{24}-Ag clusters (Figs. 2a-d). In the acquired N 1s spectra, the binding energy of Na-N and Ag-N were 399.2 eV and 399.6 eV (Fig. 2a), respectively. In the high-resolution O 1s spectra (Fig. 2b), Na-O and Ag-O bonds were observed at 532.1 eV and 532.4 eV, respectively. Notably, both Ag-N and Ag-O shifted to higher binding energies compared to those of Na-N and Na-O, respectively. The different metal-nitrogen and metal-oxygen interactions highlight the different coordination environments of Na^+ and Ag^+. These results demonstrated the successful transformation of Co_{24}-Na into Co_{24}-Ag *via* a single-crystal to single-crystal process.

The Co_{24}-Ag@Ag-NPs nanohybrid was constructed by the post-synthetic conversion of as-synthesized Co_{24}-Na to Co_{24}-Ag, followed by illumination (Fig. 1d and Scheme S1 in Supporting information). It is worth noting that Co_{24}-Ag and Co_{24}-Ag@Ag-NPs were obtained from the same reactants while undergoing crystallization and light irradiation, respectively. Inductively coupled plasma atomic emission spectroscopy (ICP-AES) indicated that the Co:Ag ratios in Co_{24}-Ag and Co_{24}-Ag@Ag-NPs are constant with the theoretical values (Table S4 in Supporting information). TG analysis showed that the final residues (Co_9S_8 and Ag) of Co_{24}-Ag (Figs. S8 and S9 in Supporting information) and Co_{24}-Ag@Ag-NPs (Figs. S10 and S11 in Supporting information) are 37 % and 48 %, re-

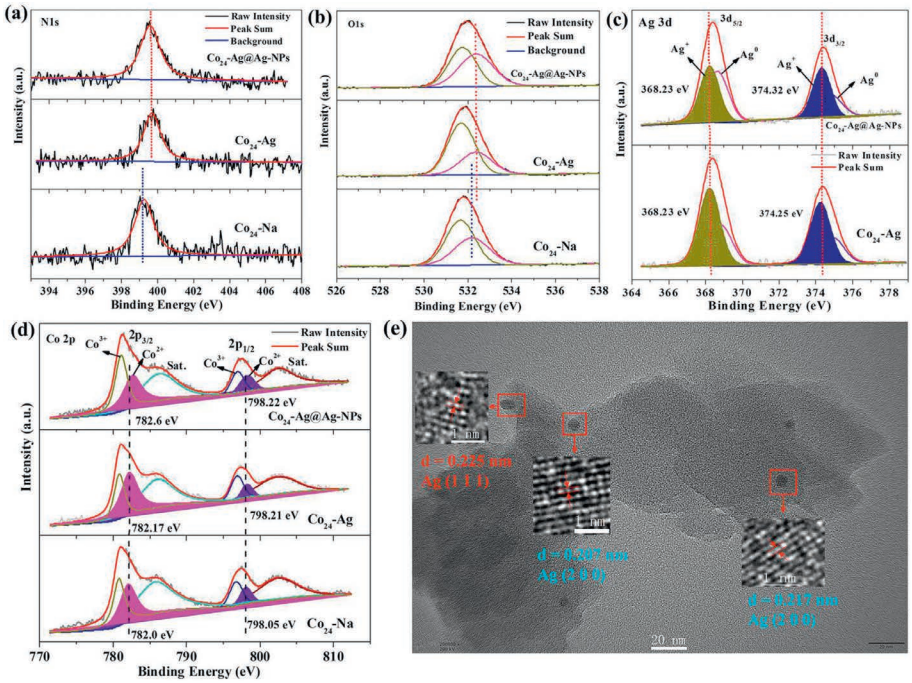


Fig. 2. (a) N 1s, (b) O 1s, (c) Ag 3d, and (d) Co 2p high-resolution XPS spectra of Co_{24}-Na, Co_{24}-Ag, and Co_{24}-Ag@Ag-NPs. (e) TEM and HAADF-STEM image of Co_{24}-Ag@Ag-NPs.

spectively, with the latter having a higher residue ratio, indicating the successful incorporation of additional Ag species beyond coordination. Transmission electron microscopy (TEM) characterization of Co_{24}-Ag@Ag-NPs showed that the Ag NPs with *ca.* 3.15 nm statistical average size were randomly distributed (Fig. S12 in Supporting information). High-angle annular dark-field scanning TEM (HAADF-STEM) images (Fig. 2e) of the species in Co_{24}-Ag@Ag-NPs showed lattice spacings indexed to the (111) and (200) planes of reduced Ag (PDF#87–0720). X-ray energy dispersive spectroscopy (EDS) mapping images of Co_{24}-Ag and Co_{24}-Ag@Ag-NPs (Figs. S13 and S14 in Supporting information) displayed that Co, S, O, N, and C were homogeneously distributed over their entire architectures, while Ag and Cl were concentrated on the specific area of the architectures. Compared with Co_{24}-Ag (Fig. S13), the Ag element dispersed on the cages and originating from the NPs was observed for Co_{24}-Ag@Ag-NPs (Fig. S14). The high-resolution Ag 3d XPS spectra of Co_{24}-Ag@Ag-NPs (Fig. 2c) disclosed the presence of Ag^+ and Ag^0. By integral calculations, the ratios of Ag^0/Ag^+ in Ag $3d_{3/2}$ and Ag $3d_{5/2}$ of Co_{24}-Ag@Ag-NPs were estimated to be 0.69 and 1.00, both of which are higher than those of Co_{24}-Ag (0.51 and 0.60). The high-resolution N 1s and O 1s spectra of Co_{24}-Ag@Ag-NPs (Figs. 2a and b) show characteristic peaks similar to those of Co_{24}-Ag, suggesting an identical Ag^+ coordination environment in the two samples. These results suggest that the Ag^+ species observed in Co_{24}-Ag and Co_{24}-Ag@Ag-NPs originated from the contribution of Ag^+ coordinated to the octahedral cages. The Ag $3d_{3/2}$ XPS peaks of Co_{24}-Ag@Ag-NPs correlated to Ag^+ slightly shifted to higher energy regions compared to those of Co_{24}-Ag (Fig. 2c). In contrast, the high-resolution Co $2p_{3/2}$ peaks associated with Co^{2+} significantly shifted to higher binding energies (Fig. 2d), indicating that a partial electron could be transferred from Co^{2+} to Ag^+ *via* coordination bonds (carboxyl μ_2-O), and then transferred to Ag-NPs under a stimulus [35,44,49]. The high-resolution Cl 2p, S 2p, and C 1s peaks were almost identical for Co_{24}-Ag and Co_{24}-Ag@Ag-NPs (Fig. S15 in Supporting information), indicating the overall consistency of the cage framework.

It has been demonstrated that thiacalixarene-based metal clusters are potential photothermal materials because their mechanism of energy release is dominated by nonradiative migration [11,38–40,50,51]. Furthermore, Ag NPs possess a noble plasmon feature with a striking photothermal effect [41–43]. Inspired by the above advantages of thiacalixarene-based metal clusters and Ag NPs, we explored the photothermal conversion properties of the obtained samples. First, we investigated the photo-responsive behaviors of Co_{24}-Na, Co_{24}-Ag, and Co_{24}-Ag@Ag-NPs. Solid-state ultraviolet-visible (UV–vis) spectra of the samples were recorded at room temperature. As shown in Fig. 3a, all samples displayed the same absorption peak at 340 nm in the UV region, which was attributed to the absorption of thiacalixarene ligands. Co_{24}-Ag exhibited higher light absorption in the range of 400–800 nm than Co_{24}-Na, indicating that the ion exchange of Na^+ with Ag^+ enabled enhanced visible light absorption. The conjugation of Co_{24}-Ag with

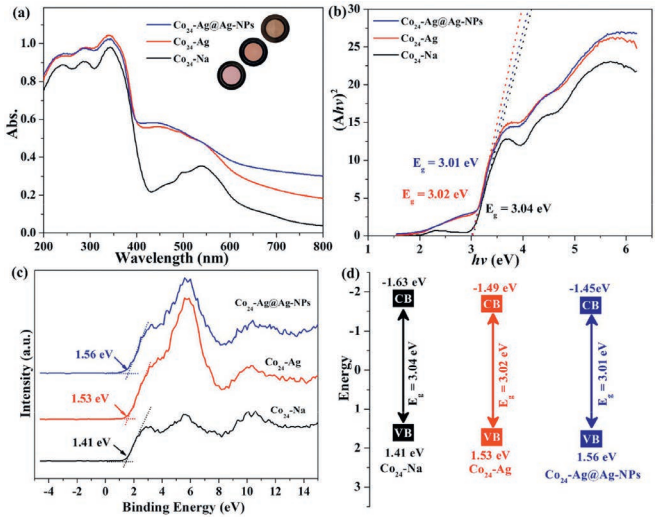


Fig. 3. Photo-responsive behavior analyses of Co_{24}-Na, Co_{24}-Ag, and Co_{24}-Ag@Ag-NPs. (a) Solid state UV–vis spectra. (b) Tauc plots. (c) Valence-band spectra. (d) The estimated VB and CB levels.

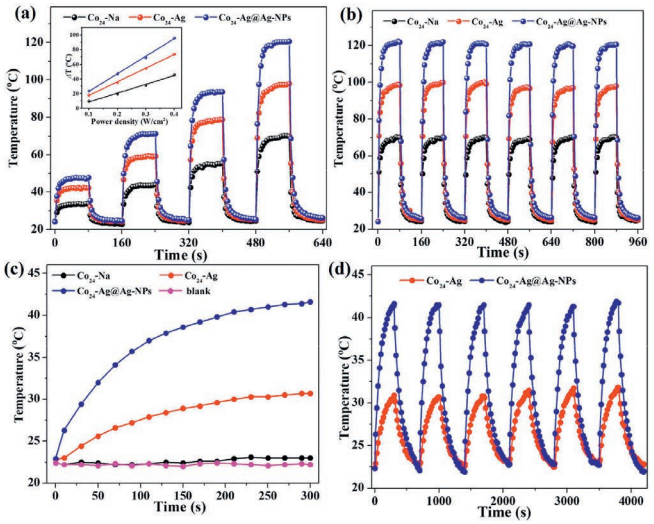


Fig. 4. (a) Time-temperature curves and (b) light on-off cycles for Co_{24}-Na, Co_{24}-Ag, and Co_{24}-Ag@Ag-NPs in the solid state. (c) Photothermal conversion curves of blank (CH_2Cl_2), Co_{24}-Na, Co_{24}-Ag, and Co_{24}-Ag@Ag-NPs in CH_2Cl_2, respectively. (d) Light on-off cycles of Co_{24}-Ag and Co_{24}-Ag@Ag-NPs in CH_2Cl_2.

Ag NPs (Co_{24}-Ag@Ag-NPs) exhibited more significant absorption in the 550–800 nm range, resulting in remarkably enhanced visible light-harvesting abilities. This result is consistent with the color changes of the samples (inset of Fig. 3a). Notably, Co_{24}-Ag@Ag-NPs showed an enhanced absorption band at ~400 nm owing to the surface plasmonic resonance of Ag NPs, which was also observed in the UV–vis absorption spectra of Co_{24}-Ag@Ag-NPs in CH_2Cl_2 (Fig. S16 in Supporting information) [52]. The band gaps (E_g, Fig. 3b) of Co_{24}-Na, Co_{24}-Ag, and Co_{24}-Ag@Ag-NPs were calculated to be 3.04, 3.02, and 3.01 eV from Kubelka-Munk function and Tauc plot, respectively. XPS analysis (Fig. 3c) revealed that the valence band (VB) potentials of Co_{24}-Na, Co_{24}-Ag, and Co_{24}-Ag@Ag-NPs were 1.41, 1.53, and 1.56 eV, respectively. According to the E_g and VB potentials, the conduction band (CB) potentials (Fig. 3d) of Co_{24}-Na, Co_{24}-Ag, and Co_{24}-Ag@Ag-NPs were calculated to be −1.63, −1.49, and −1.45 eV, respectively. The narrow bandgap of Co_{24}-Ag@Ag-NPs allows more free-charge carriers to be promoted from the VB to the CB. From these results, we supposed that Co_{24}-Ag@Ag-NPs exhibited significantly improved visible light adsorption and electron separation efficiency owing to its narrowed bandgap, which was induced by the Mott-Schottky heterojunction [52–54].

Photothermal tests of Co_{24}-Na, Co_{24}-Ag, and Co_{24}-Ag@Ag-NPs in the solid state were performed under a 660 nm lamp irradiation. Fig. 4a shows the time-temperature relationship of the samples. The temperatures of Co_{24}-Na, Co_{24}-Ag, and Co_{24}-Ag@Ag-NPs elevated with the increase of lamp power density and reached their maximum temperatures of 70.3, 97.5, and 120.4 °C at a power density of 0.4 W/cm^2, respectively. It can be observed that Co_{24}-Ag@Ag-NPs displayed the most significant temperature change, with an obvious temperature rise of ~100 °C in 1 min, followed by Co_{24}-Ag and Co_{24}-Na. No obvious decay was observed in the six on/off cycles (160 s per cycle) for the three samples under 0.4 W/cm^2 irradiation (Fig. 4b). Benefitting from its improved light capture ability and electron separation efficiency, Co_{24}-Ag@Ag-NPs exhibited superior photothermal conversion performance in the solid state.

We further performed photothermal tests of Co_{24}-Na, Co_{24}-Ag, and Co_{24}-Ag@Ag-NPs in CH_2Cl_2 solution under a 660 nm irradiation, respectively (Fig. 4c and Fig. S17 in Supporting information). As shown in Fig. 4c, no obvious temperature fluctuation was observed for blank CH_2Cl_2, demonstrating that it did not disturb the temperature response of the systems. Co_{24}-Ag exhibited an obvious temperature rise of 8.8 °C in 5 min, obviously higher than that of Co_{24}-Na ($\Delta T = 0.6$ °C) (Fig. 4c), indicating that the ion exchange of Na^+ with Ag^+ by post-modification can improve the photothermal conversion performance, which is attributed to the improved visible light absorption ability (Fig. 3a). In contrast, a distinct temperature increase of Co_{24}-Ag@Ag-NPs was detected, reaching approximately 41.7 °C (Fig. 4c). In particular, the temperature of Co_{24}-Ag@Ag-NPs at each point was higher than that of the others during the heating process, suggesting its superior photothermal conversion ability. The photothermal performance of the Co_{24}-Ag@Ag-NPs demonstrated that the Mott-Schottky junction generated by the elaborate integration of Co_{24}-Ag and Ag NPs could boost the thermal conversion performance. The photothermal stability was evaluated by reversibly irradiating and naturally cooling CH_2Cl_2 solutions of Co_{24}-Ag and Co_{24}-Ag@Ag-NPs in the light-on-off experiments. The maximum temperatures of both samples remained nearly unchanged over six cycles, demonstrating their high photothermal conversion stability (Fig. 4d). The photothermal conversion efficiency (Fig. S18 in Supporting information) of Co_{24}-Ag@Ag-NPs was calculated to be 50.2 %, which is higher than that of Co_{24}-Ag (21.6 %) and comparable with other pure Ag-based coordination complexes under similar conditions (Table S5 in Supporting information), for example, Ag30 and Ag34 [11], Ag72b and Ag28a [38], Ag16(I-IV) [55], and Ag14 and Ag43 [56]. It should be emphasized that the overall photothermal conversion performance of Co_{24}-Ag@Ag-NPs is also comparable to the representative Ag_{102} coordination clusters [57] if considering the lower Ag content (7.17 % *vs.* 46.75 %). Additionally, the visible light photothermal conversion efficiency of Co_{24}-Ag@Ag-NPs is also close to that of the bimetallic $(AgCu)_{31}$ coordination cluster [58], which makes the nanohybrid an advanced photo-responsive material, for example, used for visible light photothermal catalysts.

The Co_{24}-Ag@Ag-NPs showed high photothermal conversion efficiencies, for which the rationales could be concluded. First, Co_{24}-Ag exhibits nonradiative migration-triggered photothermal conversion behaviour. Second, Ag NPs possess inherent plasmonic localized heating characteristics. Thus, nonradiative migration and plasmonic localized heating work coordinatively to contribute to the energy release [59]. Through structural analysis, band gap measurements, and photothermal conversion tests of these samples, we derived a clear rule of thumb where Ag ion substitution (Co_{24}-Na to Co_{24}-Ag) can effectively regulate the band gap structure to enhance light absorption. The introduction of Ag NPs with inherent plasma thermal effect can form a synergistic effect with metal-thiacalixarene cage clusters (Co_{24}-Ag to Co_{24}-Ag@Ag-NPs) to increase the photothermal conversion efficiency. Therefore, the hybrid Co_{24}-Ag@Ag-NPs exhibited excellent photothermal conversion properties both in the solid state and in organic solution. It should be additionally emphasized that Co_{24}-Ag and Co_{24}-Ag@Ag-NPs were synthesized from the same starting materials, but the yield of the latter was nearly 100 %, almost double that of Co_{24}-Ag, and the photothermal conversion efficiency is also promoted by more than 2 times. From the atomic economy consideration, the preparation strategy (post-synthetic metalation) of Co_{24}-Ag@Ag-NPs has important guiding significance for the synthesis of photothermal catalyst materials, especially for the synthesis of coordination-related complexes.

In summary, the different properties of the MOCC and MNPs in the nanohybrids were cascaded to synergistically boost the photothermal conversion. Co_{24}-Ag@Ag-NPs was synthesized by ion exchange of as-synthesized thiacalixarene-based Co_{24}-Na with $AgNO_3$, followed by illumination. Co_{24}-Ag@Ag-NPs exhibited improved photothermal performance in both the solid state and organic solution. The superior photothermal performance should be

ascribed to the following factors: (1) Thiacalixarene-based Co_{24}-Ag exhibited enhanced light absorption and nonradiative migration, which can trigger photothermal conversion; (2) The plasmon nature endowed Ag NPs with notable photothermal effect; (3) The Mott-Schottky heterojunction of thiacalixarene-based Co_{24}-Ag with Ag NPs resulted in the narrow bandgap, which was responsible for the improved light capture and carrier separation efficiency, thus affecting the photothermal response; (4) The significant protective effect of thiacalixarene on the periphery of the cage clusters can effectively decrease the heat loss in the photothermal conversion process. This work highlights the significance of post-modulation involving metal substitution and the insertion of plasmonic Ag NPs on a thiacalixarene-supported Co_{24} coordination cluster to enhance photothermal performance. This study provides new insights into the design of photothermal materials visible-light applications.

CRediT authorship contribution statement

Yinjuan Guo: Writing – original draft, Investigation. **Dongao Mao:** Software, Investigation. **Kun Zhou:** Formal analysis, Data curation. **Baokuan Chen:** Validation, Funding acquisition. **Yanfeng Bi:** Writing – review & editing, Validation, Supervision, Funding acquisition, Conceptualization. **Xinxin Hang:** Writing – review & editing, Validation, Funding acquisition.

Declaration of competing interest

The authors declare that they have no known competing financial interests or personal relationships that could have appeared to influence the work reported in this paper.

Acknowledgment

This work was supported by the National Natural Science Foundation of China (Nos. 91961110, 22171122, 21901222).

Supplementary materials

Supplementary material associated with this article can be found, in the online version, at doi:10.1016/j.cclet.2025.111534.

References

[1] T.R. Cook, Y.R. Zheng, P.J. Stang, Chem. Rev. 113 (2012) 734–777.
[2] C.J. Brown, F.D. Toste, R.G. Bergman, K.N. Raymond, Chem. Rev. 115 (2015) 3012–3035.
[3] R. Ham, C.J. Nielsen, S. Pullen, J.N.H. Reek, Chem. Rev. 123 (2023) 5225–5261.
[4] Y.K. Hao, Y.L. Lu, Z.W. Jiao, C.Y. Su, Angew. Chem. Int. Ed. 63 (2024) e202317808.
[5] X.X. Hang, Y.F. Bi, Dalton Trans. 50 (2021) 3749–3758.
[6] S.K. Samanta, D. Moncelet, V. Briken, L. Isaacs, J. Am. Chem. Soc. 138 (2016) 14488–14496.
[7] J.Q. Dong, Y.T. Pan, H. Wang, et al., Angew. Chem. Int. Ed. 59 (2020) 10151–10159.
[8] D.W. Zhang, T.K. Ronson, Y.Q. Zou, J.R. Nitschke, Nat. Rev. Chem. 5 (2021) 168–182.
[9] X.Z. Li, L.P. Zhou, L.L. Yan, et al., Nat. Commun. 9 (2018) 547.
[10] Z. Wang, L. Li, L. Feng, et al., Angew. Chem. Int. Ed. 61 (2022) e202200823.
[11] Z. Wang, H. Zhao, Y.Z. Li, et al., Nano Lett. 24 (2023) 458–465.
[12] M. Yoshizawa, M. Tamura, M. Fujita, Science 312 (2006) 251–254.
[13] P. Mal, B. Breiner, K. Rissanen, J.R. Nitschke, Science 324 (2009) 1697–1699.
[14] W.D. Ward, C.A. Hunter, N.H. Williams, Acc. Chem. Res. 51 (2018) 2073–2082.
[15] X.N. Wang, P. Zhang, A. Kirchon, et al., J. Am. Chem. Soc. 141 (2019) 13654–13663.
[16] W. Zhang, M.J. Bojdys, N. Pinna, Angew. Chem. Int. Ed. 62 (2023) e202301021.
[17] H.J. Peng, J. Raya, F. Richard, et al., Angew. Chem. Int. Ed. 59 (2020) 19602–19609.
[18] G. Lu, S.Z. Li, Z. Guo, et al., Nat. Chem. 4 (2012) 310–316.
[19] Q.Q. Wang, S. Gonell, S.H.A.M. Leenders, et al., Nat. Chem. 8 (2016) 225–230.
[20] Y. Liang, X.X. Yang, X.Y. Wang, et al., Nat. Commun. 14 (2023) 5223.
[21] Y.F. Bi, S.C. Du, W.P. Liao, Chem. Commun. 47 (2011) 4724–4726.
[22] S.T. Wang, X.H. Gao, X.X. Hang, et al., J. Am. Chem. Soc. 138 (2016) 16236–16239.
[23] R.K. Gupta, Z. Wang, B. Mohan, et al., Adv. Mater. 36 (2024) 2410054.
[24] I.V. Khariushin, V. Bulach, S.E. Solovieva, et al., Coord. Chem. Rev. 513 (2024) 215846.
[25] X.Y. Chen, Q.Y. Liu, W.D, et al., Chem. Commun. 60 (2024) 11890–11898.
[26] Y.F. Bi, S.C. Du, W.P. Liao, Coord. Chem. Rev. 276 (2014) 61–72.
[27] M. Liu, W.P. Liao, C.H. Hu, et al., Angew. Chem. Int. Ed. 51 (2011) 1585–1588.
[28] X.X. Hang, B. Liu, X.F. Zhu, et al., J. Am. Chem. Soc. 138 (2016) 2969–2972.
[29] D.T. Geng, X. Han, Y.F. Bi, et al., Chem. Sci. 9 (2018) 8535–8541.
[30] H.T. Han, L. Kan, P. Li, et al., Sci. China Chem. 64 (2021) 426–431.
[31] C.X. Tan, J.J. Jiao, Z.J. Li, et al., Angew. Chem. Int. Ed. 57 (2018) 2085–2090.
[32] Y.F. Bi, X.T. Wang, W.P. Liao, et al., J. Am. Chem. Soc. 131 (2009) 11650–11651.
[33] Z.J. Guan, F. Hu, S.F. Yuan, et al., Chem. Sci. 10 (2019) 3360–3365.
[34] H.N. Qin, M.W. He, J. Wang, et al., J. Am. Chem. Soc. 146 (2024) 3545–3552.
[35] X.X. Hang, X.J. Wang, M.L. Wang, et al., Inorg. Chem. Front. 10 (2023) 926–933.
[36] X.X. Hang, B. Liu, S.T. Wang, et al., Dalton Trans. 47 (2018) 1782–1785.
[37] D.T. Geng, M. Zhang, X.X. Hang, et al., Dalton Trans. 47 (2018) 9008–9013.
[38] Z. Wang, Y.J. Zhu, O. Ahlstedt, et al., Angew. Chem. Int. Ed. 63 (2024) e202314515.
[39] Z. Wang, F. Alkan, C.M. Aikens, et al., Angew. Chem. Int. Ed. 61 (2022) e202206742.
[40] Z.H. Zhou, L.M. Xu, G.Y. Zhao, et al., Inorg. Chem. Front. 10 (2023) 3230–3236.
[41] S. Linic, P. Christopher, D.B. Ingram, Nat. Mater. 10 (2011) 911–921.
[42] P. Zhang, T. Wang, J.L. Gong, Adv. Mater. 27 (2015) 5328–5342.
[43] M. Bernardi, J. Mustafa, J.B. Neaton, S.G. Louie, Nat. Commun. 6 (2015) 7044.
[44] Y.J. Guo, J.H. Li, G.Y. Zhao, et al., Chem. Commun. 59 (2023) 5591–5594.
[45] K. Sheng, B.L. Han, Z. Wang, et al., Angew. Chem. Int. Ed. 64 (2025) e202416065.
[46] F. Hu, J.J. Li, Z.J. Guan, et al., Angew. Chem. Int. Ed. 59 (2020) 5312–5315.
[47] A. Ghosh, R.W. Huang, B. Alamer, et al., ACS Mater. Lett. 1 (2019) 297–302.
[48] T. Kajiwara, T. Kobashi, R. Shinagawa, et al., Eur. J. Inorg. Chem. 9 (2006) 1765–1770.
[49] S.L. Zhao, Y. Wang, J.C. Dong, et al., Nat. Energy. 1 (2016) 16184.
[50] Q.Q. Li, Y.H. Zou, H.R. Tian, et al., Chem. Commun. 61 (2025) 9266–9269.
[51] Q. Zhao, D.A. Mao, L.L. Huang, et al., Polyoxometalates 4 (2025) 9140091.
[52] X.Y. Lu, Z.Y. Ma, Y.N. Chang, et al., Adv. Mater. 36 (2024) 2313057.
[53] J.D. Xiao, L.L. Han, J.L. Luo, et al., Angew. Chem. Int. Ed. 57 (2017) 1103–1107.
[54] G.G. Liu, P. Li, G.X. Zhao, et al., J. Am. Chem. Soc. 138 (2016) 9128–9136.
[55] H.H. Wang, J.Y. Wei, F. Bigdeli, et al., Nanoscale 15 (2023) 8245–8254.
[56] Z. Wang, Y.J. Zhu, B.L. Han, et al., Nat. Commun. 14 (2023) 5295.
[57] Z. Wang, Y.C. Wang, C.K. Zhang, et al., Nat. Sci. Rev. 11 (2024) nwae192.
[58] L. Fang, W.T. Fan, G.Q. Bian, et al., Angew. Chem. Int. Ed. 62 (2023) e202305604.
[59] X.M. Cui, Q.F. Ruan, X.L. Zhuo, et al., Chem Rev. 123 (2023) 6891–6952.